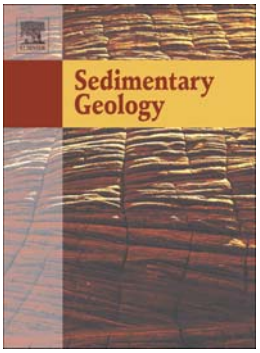

Relationship between karstification and burial dolomitization in Permian platform carbonates (Lower Khuff - Oman)

Julia Beckert, Veerle Vandeginste, Cédric M. John

PII: S0037-0738(16)30180-4
DOI: doi: 10.1016/j.sedgeo.2016.07.001
Reference: SEDGEO 5089

To appear in: *Sedimentary Geology*

Received date: 19 April 2016
Revised date: 1 July 2016
Accepted date: 3 July 2016

Please cite this article as: Beckert, Julia, Vandeginste, Veerle, John, Cédric M., Relationship between karstification and burial dolomitization in Permian platform carbonates (Lower Khuff - Oman), *Sedimentary Geology* (2016), doi: 10.1016/j.sedgeo.2016.07.001

Relationship between karstification and burial dolomitization in Permian platform carbonates (Lower Khuff - Oman)

Julia Beckert, Veerle Vandeginste, Cédric M. John

Imperial College London, j.beckert12@imperial.ac.uk

Qatar Carbonate and Carbon Storage Research Centre

Abstract

Large breccia fabrics associated with karst constitute an important structure in massive limestone successions. The dimensions and shapes of breccia structures are controlled by the initial fracture pattern of the limestone and preferential pathways of the karstifying fluids, but subsequently breccia fabrics can also govern the migration of later fluids. Therefore, breccias are highly relevant features to capture for reservoir characterisation. Outcrop analogues for Lower Khuff units in the Middle East present in the Central Oman Mountains reveal brecciated fabrics up to 10's of meters in diameter. These brecciated units are closely associated with dolomite bodies of late diagenetic origin.

Based on an integrated set of data, the breccias are interpreted as collapsed karst cavities either formed by meteoric or hypogenic fluids. The exact origin of the fluids could not be constrained due to an overprint by later dolomitizing fluids. Based on the composition of the clasts and matrix in the breccias, two dolomitization events are interpreted to have affected the succession, one prior to (early diagenetic [ED] dolomite) and one after brecciation (late diagenetic [DT2] dolomite). Dolomite of shallow burial origin (ED dolomite) was only observed as clasts within breccia and is

much more frequent than late diagenetic (medium to deep burial) dolomite clasts. Thus, the timing of the brecciation and collapse is assumed to postdate shallow burial early diagenetic dolomitization. Late diagenetic replacive dolomite (DT2 dolomite) forms 90% of the matrix in the breccia fabrics with the exception of a small area that was not affected by dolomitization, but is rarely present as clasts. Stable isotope measurements [δ^{18}O: -2.5‰ to -6‰ VPDB and δ^{13}C: 2.9‰ to 4.8‰ VPDB] suggest a burial origin for the late diagenetic dolomite potentially with the participation of hydrothermal fluids. The dolomitized matrix indicates a migration of late dolomitizing fluids subsequent to or postdating the collapse of the karstic cavities. Thus, early karstification processes seem to have played a big role in controlling subsequent loci of late dolomitization in the Oman Mountains, and potentially in other similar settings elsewhere.

Introduction

Breccia fabrics can form in various environments, and hydrocarbon reservoirs-related studies are concerned with the formational processes as well as the fluids involved in brecciation. Brecciation is often triggered by sedimentary, tectonic or diagenetic processes resulting in centimetres to hundreds of metres wide brecciated fabrics that may have contrasting petrophysical properties compared to their host rock. Large-scale breccia fabrics attracted comparatively more attention than small-scale structures in the last decades due to their impact on reservoir models. A vast majority of large-scale breccia structures has been associated with collapse of epigenetic karst structures (Hamilton and Ford, 2002; Lucia, 1995) linked to the migration of meteoric fluids in a downward direction. Recent interpretations considered also the importance of ascending fluids of non-meteoric origin defined as hypogenic karst breccias, for

instance as observed in the Middle East (Frumkin and Gvirtzman, 2006; Frumkin et al., 2015), France (Audra et al., 2010), Italy (Tisato et al., 2012), New Mexico, Texas, Nevada (Dublyansky and Spoetl, 2015) and Australia (Osborne, 2001). Often at a smaller scale, migrating warm fluids can also form breccias (Beckert et al., 2015; Frumkin et al., 2015; Hulen and Nielson, 1988) linked to hydrothermal dolomite bodies. However, breccia fabrics associated with dolomite bodies can also be of large sizes, as described for example from the Ramales platform in Spain, where breccias are related to sinistral strike slip deformation (Dewit et al., 2012). Fault controlled breccias linked to dolomite bodies have also been studied in the Zagros Mountains in Iran (Lapponi et al., 2011; Sharp et al., 2010).

The goal of this paper is to elucidate the origin of the breccia fabrics in Wadi Sahtan in the context of Middle Easterns petroleum reservoirs. Although there are hints for karstification and subaerial exposure in the Saih Hatat and in the Musandam Peninsula from Permian to Triassic times (Strohmenger et al., 2002; Weidlich, 2010), there is no evidence yet for large scale karstification in the region during Permian times. The occurrence of large-scale breccias observed within reservoir analogue, Khuff-equivalent strata at Wadi Sahtan in the Central Oman Mountains raises the question of which processes lead to their formation, and which parameters control their characteristics. In particular, this study defines the formational setting, characterises the fluids responsible for the dissolution of the host rock and evaluates potential fluid pathways as well as migration directions.

Geologic setting

Depositional and structural characteristics of the Central Oman Mountains

The Central Oman Mountains constitute an integral part of the continental Arabian plate (Searle and Cox, 1999) which stretches from the Gulf of Aden spreading axis, to the Red sea spreading centre, the Zagros-Biltis suture and to the Owen fracture zone (Stern and Johnson, 2010) in the east. The lithological succession in the Oman Mountains is represented by well-bedded layer-cake platform carbonates (Aigner and Dott, 1990; Koehrer et al., 2012; Koehrer et al., 2011). The deposition of these extensive platform carbonates was initiated from **Middle Permian to Early Triassic** times (Callot et al., 2010; Weidlich and Bernecker, 2011) triggered by the rifting of the Neo-Tethys ocean (Koehrer et al., 2011; Pillevuit, 1993; Stampfli and Borel, 2002) and the fragmentation of the supercontinent Pangaea (Ruban et al., 2007; Sharland et al., 2001). The more than 2000 km wide extension of the platform allows the study of stratigraphically equivalent sediments to Oman in the subsurface of Bahrain, UAE, Qatar, Saudi Arabia and Kuwait (Weidlich and Bernecker, 2011) (subsurface Khuff Formation). In the outcrop area in Wadi Sahtan the basement underlying the platform carbonates is of Precambrian age (Fig. 1A) with lithologies ranging from diamictites with granite boulders to siltstones, greywackes and sandstones generally known as the autochthonous Mistal Formation (Beurrier et al., 1982-1985) (Table 1). Precambrian units are separated from the Lower to Middle Permian carbonates (Saiq Formation) by an extensive unconformity present across the Central Oman Mountains (Beurrier et al., 1982-1985; Rabu et al., 1982-1983; Villey et al., 1982-1985). The Saiq Formation in Wadi Sahtan (about 640 m thick (Koehrer et al., 2010)) comprises Roadian to Changhsingian-age beds (Beurrier et al., 1982-1985; Koehrer et al., 2012; Ziegler, 2001) [some authors include Induan and partly

Olenikian-age beds in to the Saiq Formation e.g., Al-Husseini (2006) and Weidlich and Bernecker (2011) (Fig. 2B)] characterised by numerous depositional environments and lithofacies types. In detail, from Roadian to Wordian times the depositional environment is characterised by a shoal to offshoal system (Table 1). In this system, shoal to backshoal units contain microbial mats to bedded oolites and a crinoidal to peloidal shoal facies (Bendias et al., 2013). Foreshoal units comprise graded storm beds and bioclastic sheets whereas bioturbated (*Zoophycus*) mudstones are evident in the offshoal areas (Bendias et al., 2013). From Capitanian to Induan times the depositional environment is located in a more distal area of the carbonate platform and reveals tidal flat (Walz et al., 2013) as well as lagoonal sediments in addition to the back- to offshoal facies. Tempestites are also a common phenomena (Koehrer et al., 2012) (Table 1). With the beginning of Triassic times and deposition of the Mahil Formation both the Saiq and Mahil deposits were affected by a seepage reflux of hypersaline brines. In the study area, most of the middle and upper Saiq Formation (several hundreds of meters of limestone) were replaced by early diagenetic dolomite (Coy, 1997) ("ED dolomite", according to Vandeginste et al. (2015)) (Table 1). Most of the Saiq Formation in the Central Oman Mountains is replaced by ED dolomite although the base of the Saiq Formation is mostly preserved as limestone. Subsequently, from Triassic to Santonian times the carbonate succession was affected by a late diagenetic dolomitization event associated with the formation of reddish DT2 dolomite bodies (Beckert et al., 2015; Vandeginste et al., 2015) (Table 1). During Cretaceous to Neogene times the Neo-Tethys Ocean underwent closure and intra-oceanic subduction initiated in the Cenomanian which continued until the middle Turonian to early Campanian resulting in the obduction of the Semail ophiolite (Boudier et al., 1985; Breton et al., 2004; Hacker, 1994). Faulting and

folding triggered by the Alpine orogeny caused the formation of the Jebel Al-Akhdar anticline structure (Searle, 2007) at the end of the Cretaceous and allows the study of Permian outcrops in the Central Oman Mountains.

Karst and breccias in the Arabian plate

Important karst structures and breccias are present in various formations of the Arabian plate for example the Mishrif or the Sarvak formation (Cretaceous) (Botton-Dumay et al., 2002; Sharp et al., 2010). In Oman, karstification and brecciation are also of relevance during Permian to Jurassic times although only a limited number of studies are published. For example, meteoric karstification is evident in limestones in Wadi Bih on the Musandam Peninsula associated with the formation of an erosive surface including pedological features (Microcodium) (Strohmenger et al., 2002). Furthermore, the Saiq Formation in the Saiq Plateau reveals paleokarstic pockets (2 m in diameter) formed by local emersion (Baud et al., 2012). Evidences for a subaerial exposure are also present at the contact of the Saiq and Mahil Formations in the Saih Hatat (Oman) indicated by the presence of caliche hard pans (including root tubules, sheet cracks, iron staining of the matrix) and in-situ brecciation (Weidlich, 2010) (Table 1). During Jurassic times early dolomite present on the Musandam Peninsula experienced brecciation, possibly due to mass flow to gravity collapse processes . based on the intertidal to supratidal environment of deposition (Breesch et al., 2010).

Methods

One outcrop in Wadi Sahtan was mapped focussing on a large- and a small-scale breccia fabric (Fig. 2) referred to as the LSB and SSB fabric (detailed differences between both fabrics are presented in the results). The present orientation of the

analysed cliff face allows the study of a WNW-ENE oriented cross section (Fig. 2) through both the brecciated and unbrecciated Permian platform carbonates. The breccia fabrics are laterally continuously accessible. However, vertical transects across the breccia were not possible due to steepness the cliff face. The lateral extent of the breccia was determined using a measuring tape. In addition, photopanoramas were used to determine the vertical dimensions and shapes of the breccia. The stratigraphic positioning of the breccia was determined by measuring the relative distance to the *Zoophycus* horizon 2 presented by Bendias et al. (2013) in the Wadi Sahtan log. However, detailed biostratigraphic analyses were not applied to the surrounding host rock or to sampled breccia clasts.

The clast content in both breccia fabrics was obtained from image analysis by using the software ImageJ. Prior to the analysis, the field pictures were converted into an 8bit grayscale image. Subsequently, the images were analysed with the threshold method "Default" by applying an HSB colour space. By adapting the brightness level a clear separation between matrix and clasts was achieved which allowed the calculation of the relative percentage of each phase. The result was compared with the total amount of pixel in the picture.

Hammer and chisel were used to collect 150 representative samples of the breccia body as well as of the surrounding host rock. In order to determine the presence and arrangement of iron rich and iron poor dolomite and calcite phases, all hand samples and thin sections were stained following the following modified procedure of Dickson (1966). Hand samples were etched for 30 seconds by using a 1M HCl solution prior to staining. The staining solution was prepared by about 500 ml of distilled water, 2.5 ml concentrated HCl, 0.6 g of Alizarin Red S and 8 g of Potassium hexacyanoferrate III.

The reaction time of hand samples with the staining suspension was set to 30 seconds, whereas 20 seconds was applied for thin sections.

The Zeiss Axioskop 40 microscope was used to analyse 12 30µm-thick thin sections under transmitted light followed by capturing image sections with a Zeiss AxioCam ICc1 camera.

The elemental analysis of limestones and dolomite types was achieved by using a handheld Bruker Tracer IV-SD (ED-XRF). The device uses a rhodium target as well as a Silicon Drift Detector to allow the detection of lighter elements. The operational voltage was set to 40 kV for Trace Mud Rock (TMR) measurements and 15 kV for Major Mud Rock (MMR) analysis. TMR measurements were conducted on manganese, iron, zinc, rubidium, strontium and barium whereas magnesium, calcium, silicium and potassium have been measured with MMR. Elemental results were obtained from polished surfaces of hand samples under vacuum conditions (Bruker 3V Vacuum Pump). A correction of mudrock calibrated XRF values was undertaken for carbonate by applying the carbonate correction equations published by Quye-Sawyer et al. (2015).

Stable isotope analysis focused on potential variations in the oxygen isotopic signature of the dolomite matrix along a lateral transect across the LSB fabric (yellow dashed line in Fig. 2A). Carbon and oxygen stable isotope results were obtained from 90 to 150µg sample powder of 18 samples. The sampling procedure focussed on matrix dolomite and aimed to avoid veins, fractures or fossils. The micro-sampling approach was achieved by the use of a dental drill. Stable isotope analysis were performed using a Thermo Scientific Kiel IV carbonate device coupled to a MAT253 mass spectrometer in the Qatar Stable Isotope Laboratory at Imperial College London. Powdered samples were reacted with phosphoric acid at 70°C. Analytical

reproducibility was checked by replicate measurements of an internal laboratory standard (Imperial College Carrara marble δ^{13}C value of +2.09‰ and a δ^{18}O value of -2.03‰) with a standard deviation of up to 0.03‰ for δ^{13}C and up to 0.08‰ for δ^{18}O. In addition, 5 samples were measured three times on a regular basis to ensure sample reproducibility (standard deviation of up to 0.1‰ for δ^{13}C and up to 0.05‰ for δ^{18}O). All oxygen isotope results derived from dolomite were corrected for acid fractionation by applying the fractionation factors published by Rosenbaum and Sheppard (1986) and Kim et al. (2007) [(1.0087*(1000 + corrected δ^{18}O) / (1.00992641-1000)]. All carbon and oxygen isotope results presented in the text are given in per mil relative to the Vienna Peedee Belemnite (VPDB).

Results

Two breccia fabrics are present in the studied outcrop in Wadi Sahtan (Fig. 1) defined as a small-scale breccia fabric (SSB) and a large-scale breccia fabric (LSB) (Fig. 2). The LSB and SSB fabrics never touch, and occur as laterally separated units.

Dimensions and shape of the brecciated areas

The LSB fabric extends laterally up to 90 m and has a maximum thickness of 40 m measured in a bedding perpendicular direction (Fig. 2). In comparison, the extent of the SSB fabric is smaller than the LSB fabric with 10 m in width and 15 m in height (Fig. 2). The shape of both breccia fabrics varies with respect to the edges of the brecciated areas. The LSB fabric exhibits sharp and straight edges parallel to one bedding plane at the top as well as bedding perpendicular edges on both sides (Fig. 2). The base of the central part of the LSB fabric is covered by scree, so no observations can be reported from that zone. The shape of the SSB fabric is more irregular and can

be described as brecciated zones characterized by a pipe shape extending away from the central part of the SSB fabric towards stratigraphically older beds (Fig. 2).

Non-brecciated areas are locally present in between the two brecciated pipe-shaped areas at the base of the SSB fabric (Fig. 2). The top of the SSB fabric reveals a transitional contact zone from a highly brecciated fabric towards a dolomitized zone lacking any brecciation features (Fig. 2) or clasts floating in a matrix.

Stratigraphic position of the breccia fabrics LSB and SSB

The brecciated interval is located in lower Permian platform carbonates stratigraphically equivalent to lower Khuff units present in the subsurface of Qatar (Table 1), the United Arab Emirates and Saudi Arabia. In comparison with the mapping results of Bendias et al. (2013) the base of the SSB fabric is cross cutting *Zoophycus* horizon 2 whereas the top is located 21 above this bioturbated layer. The top of the LSB fabric is roughly located 40 m above *Zoophycus* horizon 2 and located in limestone beds of Wordian age. Due to scree coverage the lowermost base of the LSB fabric is not exposed and thus, a specific stratigraphic interval could not be defined.

Characteristics of clasts present in the LSB and SSB breccia fabric

LSB Fabric

The brecciated area shows two different zones with respect to the clasts size and appearance. The outer parts of the LSB fabric are defined as area 1 (Fig. 2). The clasts range in size from 1 cm to 40 cm and reveal angular shapes (Fig. 3A and B). The central part of the breccia defined as area 2 is characterized by centimetre to tens of meter sized blocks (Fig. 2 and 3E) and clasts of up to 35 cm in diameter. Some blocks

reveal similar bedding plane directions as the surrounding host rock and lack evidence for a displacement. The shape of the clasts is angular.

The composition of clasts is similar in area 1 and 2, with two different types of clasts. The first type exhibits brownish weathering colours and is fabric preserving. Shell debris, crinoids or fusulinid foraminifera are still recognizable. The finely crystalline texture is characterised by subhedral planar-s dolomite rhombs of 10 to 30 μm crystal size. The first type of dolomite is, based on it's fine crystalline fabric preserving texture and the brownish colour, similar to early diagenetic dolomite described by Coy (1997) (referred to as D2 dolomite) and ED (early diagenetic) of Beckert et al. (2015).

In comparison, the second type of clasts consists of fine to medium dolomite rhombs ranging from 15 to 140 μm with inequigranular idiotopic to hypidiotopic crystal shapes (Fig. 3F and G). The planar-s dolomite fabric is tightly packed. Mosaic extinction was rarely observed in association with subhedral dolomite crystals. Due to similarities in field and petrographic characteristics with DT2 dolomite of Beckert et al. (2015) and observations of Coy (1997) (described as D3 and D4 dolomite) the second type of clasts is defined as DT2 dolomite. ED clasts dominate the clastic fabric (Fig. 3G) but the content of DT2 clasts is slightly increased in the ENE part of area 1.

SSB Fabric

In contrast to the LSB fabric, the SSB fabric is characterized by the presence of limestone, ED and DT2 clasts. The clasts range in size from 0.5 cm to 25 cm and have very angular to angular shapes.

The amount of clasts decreases towards stratigraphically younger beds and the fabric changes from clast to matrix supported. The topmost part represents a transition zone into a DT2 dolomite body. Several clasts reveal stylolites oriented in different

directions ranging from bedding parallel to nearly bedding perpendicular (Fig. 4E). At the base and in the centre of the breccia up to centimetre wide areas lack brecciation features and are preserved as limestone (Fig. 4C and D). Preserved bedding planes within these limestone areas reveal bedding directions similar to the non-brecciated host rock and lack any evidences for a displacement. Centimetre-wide nearly bedding parallel pipes filled with clasts connect brecciated areas across non brecciated limestones (Fig. 4F).

Characteristics of the matrix present in the LSB and SSB breccia fabric

LSB

The brecciated fabric is characterized by a dark red DT2 dolomite matrix (Fig. 3A and C). The preservation of fossils is generally very poor. Diagenetic fabrics such as zebra structures are not present. Fractures revealing DT2 dolomite halos with increasing width towards stratigraphically younger beds occur at the base of the breccia (Fig. 5A). Vugs with a maximum diameter of 0.5 cm are rarely observed in the matrix characterised by coarse dolomite crystals at the edge and blocky calcite in the centre (Fig. 5B).

SSB

The matrix present in the SSB fabric is not dolomitized at the base and in the centre and changes gradually into DT2 dolomite towards the breccia top and the edge (Fig. 4C and D). The most striking difference to the LSB fabric form finely laminated limestone layers with a maximum lateral extent of 30 cm and a thickness of 15 cm (Fig. 5C). The laminae contain abraded crinoid debris alternating with fine crystalline mudstone laminae. In comparison, the matrix of the unbrecciated limestone host rock shows well-preserved fossils. The faunal assemblage ranges from crinoids, to

gastropods, bivalves, rugose and tabulate corals, fusulinid foraminifera and bryozoans (Fig. 5D). Bioturbated layers (*Zoophycus)* reveal sharp boundaries with the limestone matrix of the SSB breccia fabric (Fig. 5E). In addition, dolomitized celestite laths occur within and around the SSB fabric (Fig. 5F).

Picture based clast analysis

Picture based area calculation analysis were applied to two pictures of the LSB and two of the SSB fabrics presented in Figure 3 and 4 in order to evaluate the relative ratio between clasts and matrix. The results of the LSB fabric reveal a clast/matrix ratio of 44/56% for Fig. 3B and a ratio of 51/49% for Fig. 3D. Only images from the base and the centre of the SSB fabric were analysed. The results reveal a clast/matrix ratio of 51 to 49% for Fig. 4B and 68 to 32% for Fig. 4D. Thus, the clasts occupy a larger volume in the SSB fabric.

Stable isotope analysis

The results show clusters in the stable oxygen versus carbon plot related to different areas in the LSB fabric. DT2 dolomite samples taken within the dolomite fingers (Fig. 6A) have relatively similar carbon and oxygen isotope values (Fig. 6A dark gray area) [δ^{18}O deviate on average by a maximum of 3.5‰ VPDB and δ^{13}C by a maximum of 2‰ VPDB]. Thirteen DT2 dolomite samples taken within the matrix of the LSB fabric reveal similar values to the dolomite fingers [δ^{18}O: -2.5‰ to -6‰ VPDB and δ^{13}C: 2.9‰ to 4.8‰ VPDB]. However, the centre and the edges of the LSB fabric show more positive carbon and oxygen values (Fig. 6A light gray area) [δ^{18}O: -2.42‰ to 0.6‰ VPDB and δ^{13}C: 4.6‰ to 6.2‰ VPDB].

The spatial variation of the values present in the DT2 dolomite clusters is best visible along a transect across the LSB fabric including the non-brecciated dolomite rimming

the breccia (Fig. 6B). The outer edges of area 1 and 2 of the LSB fabric show $\delta^{18}O$ values of 0.6 to -2.42 (‰ VPDB) compared to the $\delta^{18}O$ signature of -2.5 to -6.0 (‰ VPDB) of the dolomite fingers extending away from the breccia (Fig. 6B). The carbon isotopic signature shows more negative values of about 3.5‰ VPDB in dolomite fingers rimming the breccia and more positive values of about 6‰ VPDB inside the breccia body. However, several excursions in the carbon isotope signature within the unbrecciated dolomite fingers reach nearly similar values as the samples in the breccia matrix. Oxygen and carbon isotopic values seem to co-vary (Fig. 6B).

XRF elemental analysis

The amount of magnesium and calcium present in the DT2 dolomite matrix of the LSB fabric is relatively homogenous ranging from 9.5 to 13.2 % (± 1.1 %) for magnesium and 22.9 to 23.9 % (± 0.2 %) for calcium. Different magnesium and calcium values were only measured in the large limestone blocks occurring in area 2 with 3.0 % (± 0.2 %) and 25.2 % (± 0.2 %) respectively. A slightly increased silica content of 1.4 % (± 0.02 %) was recorded in area 1 in the LSB fabric compared to 0.3 % (± 0.01 %) in area 2. Furthermore, the potassium content increases from area 2 (0.1 % ± 0.04 %) towards the WNW into area 1 (0.3 % ± 0.01 %). The highest manganese content has been recorded in the ENE part of area 1 with 5108 ppm (± 177.8 ppm) compared to 471 ppm (± 26.9 ppm) in area 2. The iron content is variable and lacks a trend. The non-brecciated DT2 dolomite fingers extending away from the LSB fabric are characterised by significantly increased manganese contents of up to 9702 ppm (± 316.4 ppm) compared to the LSB and SSB fabric. Calcium, magnesium and iron in the dolomite fingers are comparable to part 1 in the LSB fabric.

The SSB fabric reveals locally increased values of calcium (up to 27.1 % (± 0.2 %)), manganese (6837 ppm (± 229.7 ppm)) and zinc (up to 291 ppm (± 14.8 ppm)) in comparison with the LSB fabric.

Discussion/ Interpretation

Two potential timings ([1] synsedimentary to shallow burial and [2] medium to deep burial) were considered as possible for the formation of the LSB and SSB fabrics. The synsedimentary to shallow burial timing would imply formation of the LSB and SSB fabrics ranging from the deposition of lower Permian beds until the Wordian age based on the age of the strata hosting the breccias. The second interval defined as medium to deep burial ends presumably with the emplacement of the ophiolite during the Cretaceous, based on the dolomite phases present.

Synsedimentary to shallow burial origin of the breccia

A synsedimentary origin of the breccia fabric could be associated with mass flow deposits caused by grain or debris flows and turbidity currents. However, several facts make a synsedimentary origin of the LSB and SSB breccia fabric improbable. Firstly, the limestone bed above the LSB fabric has a very sharp and straight contact with the underlying breccia and an uneven base would be expected for the first laterally continuous bed deposited above a mass flow deposit. In addition, the presence of tens of metres wide blocks in area 2 of the LSB fabric which lack a displacement and non-brecciated zones in the SSB fabric contradict an interpretation as mass flow deposit. Secondly, the depositional environment for this interval of the Khuff was interpreted as a shallow dipping carbonate platform with a gentle topography (Koehrer et al., 2012), several kilometres away from the platform margin (according to the

paleofacies map of Ziegler (2001)). There is no evidence for wide and deep channels or mass flow deposits in the well-bedded carbonates of Lower Permian age in Wadi Sahtan. Thirdly, the angular clasts lack any signs of longer transport, which would result in more pronounced rounding.

A second mechanism for a shallow burial origin of the breccia would be the formation of surficial karstic features such as e.g. collapsed sinkholes. This can be excluded due to the absence of the characteristic subaerial regolithic cover sediments (Salvati and Sasowsky, 2002). Instead, the top of the LSB breccia fabric is characterised by a straight marine carbonate bed that can be traced over several hundreds of meters. A shallow burial origin of the breccia is furthermore not likely due to the presence of both the early and late diagenetic dolomite observed in clasts. DT2 dolomite was formed during burial (Beckert et al., 2015) postdating initial pressure solution. Therefore, a medium to late diagenetic origin of the breccia is assumed supported by stylolite orientations in the clasts of the SSB fabric that deviate erratically from orientations measured in the surrounding host rock. This implies a stylolite formation prior to brecciation and thus, contradicts a shallow burial origin. Thus, a shallow burial or synsedimentary origin of the breccia fabric with subsequent dolomitization and recrystallization of clasts as observed in brecciated outcrops at the Musandam Peninsula (Breesch et al., 2010) can be excluded.

Medium to deep burial origin of the breccia

Tectonic abrasion, dissolution of evaporitic layers and subsurface karstification are most likely to be of relevance in this setting, and field and geochemical characteristics of the breccia fabrics can help to determine which mechanism was responsible for their formation.

A pure tectonically related mechanical diminution or abrasion scenario (Jébrak, 1997; Keulen et al., 2007; Mort and Woodcock, 2008; Wright et al., 2009) can be excluded due to the absence of intensive faulting, shearing and shear bands as well as clasts yielding striations. In addition, limestone beds above the LSB fabric lack displacements contradicting the presence of an extensive fracture zone. Furthermore, although there are lots of faults and fractures in the region, none of the faults reveal gouges with long deformation bands linked to the formation of tens of meter wide breccia structures as present in Wadi Sahtan. The pipe-to-finger shape of the SSB fabric does not indicate a fault gouge setting. This is supported by vertical variations in the clast/matrix content in the SSB fabric whereas fault gouges often reveal extensive crackling up processes of beds rimming a vertical fracture zone in lateral direction away from the fracture plane.

Another scenario comprises the dissolution of local patches of sulphates which requires a brine density flow (Anderson and Kirkland, 1980) triggered by pressurized meteoric water exploring a present fracture system. The potential presence of some sulphate minerals is supported by the presence of celestite laths within and next to the SSB fabric. However, a primary deposition of sulphates, for example linked to extensive evaporation, can be excluded due to the fully marine record of the deposited Middle Permian sediments indicated by crinoids, rugose corals and fusulinids. Thus, only allochthonous sulphate intrusions are conceivable, potentially sourced from Ediacaran-Cambrian evaporites that were primarily deposited along the northern margin of Gondwana (Husseini and Husseini, 1990; Smith, 2012). A regional complication for this scenario though is that the evaporitic layers of the Ara salt in Oman occur in the Huqf and Dhofar area and do not underlie Permian strata in the Central Oman Mountains (based on the salt basin distribution map of Smith (2012)

and Reuning et al. (2009)). Therefore, the dissolution of tens of metres wide patches of evaporites followed by a collapse and brecciation of overlying units is also not considered as a realistic scenario.

Due to the high amount of large scale dolomite bodies related to karst systems in the Middle East e.g., hosted in the Cretaceous Sarvak formation in Iran (Hajikhazemi et al., 2010; Lapponi et al., 2011; Sharp et al., 2010), the Bih formation in the United Arab Emirates (Fontana et al., 2010) or the Hiyam Formation exposed in the Saih Hatat (Chauvet et al., 2009), a karst origin of the breccia is considered here. This could be related to the involvement of hydrothermal, hypogenic or meteoric fluids in the formation of karst cavities in the studied outcrop section.

Firstly, a hydrothermal karst origin of the observed breccia fabrics potentially linked to H_2S as described by Hill (1990) is considered implausible. A hydrothermal control on the karst formation requires warm ascending fluids. The presence of dolomite clasts and matrix comparable to dolomite bodies described in Vandeginste et al. (2015) and Beckert et al. (2015) with respect to field characteristics and stable isotope results could potentially indicate the ascent of warm dolomitizing fluids resulting in karst cavities. However, the breccia matrix of the SSB fabric is partly composed of undolomitized limestones and thus, migrating warm dolomitizing fluids were not involved in the formation of the breccia matrix. Furthermore, the absence of typical hydrothermal karst features such as veins or crystal lined vugs as observed e.g., in Hungarian karst systems (Dublyansky, 1995) make a hydrothermal karst system unlikely. Classical indicators of high temperatures such as zebra fabrics or saddle dolomite are also missing in the outcrop.

A secondly potential scenario involves ascending fluids arrested in their movement resulting in a so-called hypogenic type of karst, a process well documented in the

Middle East for example from Israel (Frumkin et al., 2015) or Saudi Arabia (Kempe et al., 2009b). The straight and vertical orientation of the edges of the LSB fabric coincides with observations in other hypogenic caves such as in Jordan (Kempe et al., 2009a) potentially representing vertical shafts. In Wadi Sahtan the nearly horizontal pipes in the SSB fabric and the partly non-displaced blocks in area 2 of the LSB fabric constitute an indication for network structures in a hypogenic or meteoric setting. However, the most emblematic features of hypogenic caves, i.e. network mazes or spongework mazes (Klimchouk, 2011) potentially present before brecciation, are not preserved.

Thirdly, the possibility of a meteoric karst system was examined. In order to assess the assumed meteoric karst formation of the SSB and LSB fabric in more details, the clast to matrix ratio were compared with the diagram from Woodcock et al. (2006). The ratios of the LSB breccia fabric indicate a matrix to cement supported chaotic breccia fabric. Due to the decrease of clasts from the base to the top observed in the SSB fabric a trend from a matrix/ cement supported chaotic breccia fabric to a cave sediment with chips and blocks can be interpreted. This supports the potential presence of a subsurface meteoric karst system. However, a subsurface meteoric karst system requires the presence of meteoric water exploiting pathways that allow fluid exchange with the surface. Evidences for a temporary subaerial exposure of Upper Permian to Early Triassic carbonate beds are presented by Koehrer et al. (2012) incorporated in the lithofacies type "burrowed to vertically rooted mudstone to wackestone" deposited in a backshoal setting in the study area. These carbonate sediments occur several tens of metres above the studied breccia fabrics and require a fluid exchange potentially along fracture planes although no long fracture planes are exposed in the outcrop. However, fluid and sediment exchange with the surface is

evidenced by stratified sediments in the matrix of the SSB fabric containing crinoidal debris.

Characterization of fluids and fluid flow mechanisms

Observed dolomite phases:

ED dolomite is associated with the migration of mesosaline brines present in a seepage reflux setting (Vandeginste et al., 2013). The direction of migration of fluids is thus defined as downwards to slightly lateral. Early dolomitizing fluids are expected to have entered the succession during shallow burial and predate most likely the karstification. This is derived from the fact that most of the clasts are formed of ED dolomite. Brecciation of early dolomitized limestones in the Middle East has for example been observed in Jurassic carbonates on the Musandam peninsula (Breesch et al., 2010).

In the study area in Wadi Sahtan DT2 dolomite is considered as late diagenetic in origin and linked to the ascent and lateral migration of presumably warm fluids (Beckert et al., 2015; Vandeginste et al., 2015). The ascending nature is indicated by the increasing width of dolomite halos around fractures towards stratigraphic younger beds observed at the base of the breccia fabrics. These features could be interpreted as small scale christmas tree structures or decimetre scale dolomite plumes associated with fluid migration, similar to what was observed in Iran (Sharp et al., 2010). Christmas tree patterns have also been recognized in other dolomite bodies such as in Spain (López-Horgue et al., 2010) and in more eastern areas of the Jebel Akhdar tectonic window (Vandeginste et al., 2013).

The locally more positive $\delta^{18}O$ values measured in the breccia matrix of the LSB fabric could arguably be interpreted to represent either: 1) mixing of fluids with

different temperatures, or 2) a replacement of early by late dolomite. These assumptions are based on the fact that the oxygen isotopic composition of the dolomite depends on the precipitation temperature and the isotopic composition of the parent fluid (Hoefs, 2004). In the studied outcrops the last assumption is assumed to be the most likely one. The replacement of early (ED) by late diagenetic dolomite (DT2) in the Central Oman Mountains has been described by Beckert et al. (2015) for other outcrops of similar age. In addition, results of McKean (2012) show $\delta^{18}O$ values of -3.24 to -0.74 ‰ (VPDB) and $\delta^{13}C$ values of 6.31 to 6.48 ‰ (VPDB) for ED dolomite. This is consistent with results of early diagenetic dolomite measured by Coy (1997) ($\delta^{18}O$: -4 ‰ to 1 ‰ VPDB and $\delta^{13}C$: 3 ‰ to 6 ‰ VPDB) defined as pervasive D2 dolomite. The comparison of ED and DT2 dolomite [$\delta^{18}O$: -2.5‰ to -6‰ VPDB and $\delta^{13}C$: 2.9‰ to 4.8‰ VPDB] shows more positive oxygen and carbon values for ED dolomite (Fig. 6A). Thus, a replacement of ED by DT2 dolomite and potential mixing of phases in one sample would result in the observed trend presented in Fig. 6. A similar trend of oxygen isotopes linked to the replacement of early by late dolomite has also been observed by Breesch et al. (2010) on the Musandam Peninsula.

Although the replacement of ED by DT2 dolomite is the preferred scenario a mixing of multiple fluids at different temperatures associated with variable $\delta^{18}O$ values could also result in the observed isotopic trend. This scenario is supported by the absence of diagenetic fabrics such as vugs or zebras in areas with more positive oxygen values whereas more negative oxygen values (i.e. warmer fluids) were observed in the dolomite fingers. Saddle dolomite and zebra dolomite textures are common features in these dolomite fingers indicating temperatures above 60°C (Radke and Mathis, 1980; Spötl and Pitman, 2009). Due to the lack of measureable fluid inclusions in thin

sections, exact dolomite formation temperatures could not be obtained. In addition, the deep burial around Cretaceous times triggered recrystallization which impacted clumped isotope temperatures (Vandeginste et al. (2014). However, in case of a mixing of multiple fluids it can be assumed that the elemental composition of these fluids is relatively similar due to a lack of elemental variations between the centre (area 2) and the edge (area 1) of the LSB breccia fabric. The contents of magnesium and calcium are similar plotting around 11 % and 23 % respectively. Deviations of less than of 0.1 % were also determined for silicium, potassium and iron. The strontium content is about 10 ppm lower in area 2 comparing to area 1 even though this difference is negligible.

Fluids associated with the karstification:

Based on evidences from the characteristics of the clast and matrix within breccias, early and late diagenetic dolomitizing fluids are not considered as relevant to the karstification. Thus, a third fluid is assumed to be responsible for the cavity formation. In many hypogenic carbonate hosted cave systems, besides the temperature and the ionic strength of the solution, the content of CO_2 and H_2S are postulated as important factors to trigger dissolution (Dublyansky, 1995, 2000). However, a dominant presence of H_2S in the karstifying fluid remains unlikely due to the absence of sulphuric minerals like sphalerite, galena or marcasite in the outcrop. The enrichment of fluids in CO_2 in hypogenic settings demands either thermometamorphism of carbonates, or oxidation as well as thermal degradation of organic compounds by mineral oxidants or igneous processes (Klimchouk, 2011). Thermal metamorphism can be excluded due to the absence of a magma body rimming the platform carbonates. This is supported by the absence of a characteristic

isotopic signature (e.g., $\delta^{18}O$ lower than -22‰ as shown for hydrothermal carbonates by Horton et al. (2012)) expected to be present in case of the involvement of magmatic fluids. However, this is highly dependent on the rock/ fluid ratio and a high rock/fluid ratio could imply a closed system recrystallization. Igneous processes as well as the migration of hydrocarbons required for thermal degradation have not been proposed regionally during Triassic to Cretaceous times.

Thus, a hypogenic source of fluids rich in H_2S or of magmatic origin appears less likely compared to the migration of meteoric fluids. In addition, due to the absence of evidence for flow charge and discharge, the reconstruction of pathways or directions of flow proves to be complicated.

Proposed model for the formation of the breccia fabrics

The interpreted conceptual model of formation of the LSB and SSB fabrics has been subdivided into six stages presented in Fig. 7. Based on the aforementioned discussion only meteoric and hypogenic karstifications are considered as potential processes resulting in cavity formation followed by collapse.

The deposition of platform carbonates during Lower to Middle Permian times represents the first stage (Fig. 7A). During shallow burial, lithification and initial compaction potentially triggered the formation of fractures in the succession. Linked to seepage reflux of mesosaline brines, limestone replacement by a finely crystalline and fabric preserving dolomite (ED dolomite) took place (Beckert et al., 2015; Vandeginste et al., 2015). The migration of these early diagenetic dolomitizing fluids terminates at the end of this stage.

The second stage (Fig. 7B) comprises the migration of karstifying fluids through the succession most likely during medium burial. The timing was firstly derived from the

vertical edges of the LSB fabric presumably linked to tens of metres long fracture planes that are expected to postdate shallow burial. The direction of fluid flow is either directed downwards (meteoric fluids) or upwards (hypogene karst formation). Due to the presence of transported crinoid debris within the limestone matrix of the SSB fabric in between non-displaced blocks a meteoric karst system is more likely (descending transport direction). Major fluid pathways are typically fracture planes cross cutting bedding planes and thus, forming a network. Secondly, the presence of ED clasts in the LSB and SSB fabric indicates a migration of karstifying fluids postdating the formation of early dolomite by seepage reflux of saline brines during shallow burial. Thirdly, the assumed meteoric origin of the karst system requires fluid pathways connected to the surface during times of subaerial exposure. Evidences for subaerial exposure are provided by Koehrer et al. (2012) during Triassic times, which implies medium burial conditions for beds deposited during Middle Permian times. During this stage the formation of cavities is initiated due to the migration of karstifying fluids.

The lateral and vertical extension of the cavities (Fig. 7C) is progressively widened by dissolution during the third stage. Due to the large amount of ED clasts in the LSB fabric it can be assumed that a direct contact zone between karst cavity and the base of ED dolomite was developed. However, a replacement of potential limestone clasts by dolomite cannot be excluded. An irregular box work fabric of cavities is assumed based on the occurrence of large non-displaced blocks in the LSB fabric and narrow nearly vertical pipes in the SSB fabric. The non-diplaced blocks acted as pillars in between the cavities and stabilized the karst system.

During stage four the collapse of the cavities is most likely initiated (Fig. 7D) resulting in the formation of clast filled cavities. A collapse scenario is supported by

the clast appearance and the relative clast/matrix ratio compared to the diagram of Woodcock et al. (2006). The presence of the large blocks in area 2 indicates the preservation of pillars in the centre of the cavern. The matrix of the breccia is most likely composed of carbonate sediment characterised by an increased porosity. That provides additional pathways for migrating late diagenetic dolomitizing fluids resulting in the matrix being replaced by DT2 dolomite. This second type of dolomitizing fluids (DT2 dolomite) migrates upwards through the succession following major fractures and the pre-existing karstic system (Beckert et al., 2015; Vandeginste et al., 2015). ED clasts are presumably recrystallized by DT2 dolomite up to a certain extent.

The last stage (Fig. 7E) is characterized by the dolomitization of LSB fabric and the formation of tens of meters wide dolomite fingers extending laterally away from the breccia. Due to the presence of DT2 clasts in a limestone matrix at the base of the SSB fabric it is assumed that the breccia formation postdates the recrystallization of the units above the SSB fabric by DT2 dolomite.

Conclusion

The Middle East hosts a large number of brecciated structures observed in platform carbonates and salt deposits. Traditionally, their origin was mainly linked to epigenetic fluid migration whereas the importance of hypogenic processes for the region received more attention only during recent years. This study aimed to provide a detailed analysis of the presence of dolomitizing and karstifying fluids examined in tens of metres wide breccia fabrics in a stratigraphic interval equivalent to the Lower Khuff in the Central Oman Mountains. The breccias are hosted in Lower Permian carbonates of the Arabian plate which were exposed to two different dolomitizing

fluids as well as a fluid that caused the formation of karst cavities. Within the breccia fabrics, the first type of dolomite (ED dolomite) was mainly observed in clasts whereas the surrounding host rock constitutes of extensive ED dolomite from Permian to Triassic beds. Mesosaline brines are assumed to be the dolomitizing fluids for ED during shallow burial (Vandeginste et al., 2013), and based on field characteristics dolomitization is interpreted to predate karstification. During medium burial what was most likely a maze pattern karstification was initiated, triggered by the migration of either meteoric or hypogenic fluids. The geochemical signal required for the clear separation of both processes is not clear due to a later recrystallization event during and subsequently to the emplacement of the ophiolite. However, a meteoric karst process is the favoured interpretation based on evidences for cave sediment (derived from the diagramm of Woodcock et al. (2006) defined for chaotic breccias in England) and evidences for early marine sediment transport from the surface (laminated sediments rich in crinoid debris observed in the breccia matrix). Subsequent to the collapse of the karst cavities a second ascending dolomitizing fluid (late diagenetic DT2 dolomite) is thought to have entered the brecciated area. The warm fluids recrystallized large parts of the matrix and to a minor extent clasts, as indicated by a trend in the carbon and oxygen isotopes. Due to the relative timing of karstification and later dolomitization by DT2 dolomite, the formation of cavities is assumed to predate the emplacement of the ophiolite in Oman. This scenario, which links epigenic karst with burial dolomitization, implies that the spatial distribution of dolomite bodies will follow the template of karstic conduits. If this interpretation is correct, it implies that a geostastical predictive model can be derived for the distribution of late diagenetic dolomite bodies by using typical variograms for the distribution of karstic features.

Acknowledgements

This research project is funded by Qatar Petroleum, Shell, and the Qatar Science and Technology Park. We thank Marijn van Capelle and Catriona Reynolds for their help during field data acquisition and sampling. We also thank the Shuram Oil and Gas Logistics branch for providing logistical support during field work. We acknowledge editor Brian Jones and the reviewers for their constructive comments, which helped improve this paper.

Table captions

Table 1: The table summarizes sedimentological characteristics (Bendias et al., 2013; Koehrer et al., 2012; Walz et al., 2013) of the study area listed in chronological order (chronology based on Al-Husseini (2006)). In addition, the timing of dolomitization is shown as well as brecciation and karstification events observed across the Arabian plate.

Table 2: The table presents concentrations of elements measured in samples of the LSB and SSB fabric obtained with the XRF tool.

Figure captions

Fig. 1: [A] The geological map shows the distribution of Upper Proterozoic to Middle Cretaceous units in the Jebel Akhdar tectonic window located in the Central Oman Mountains. The studied outcrop is located in Wadi Sahtan (red box). [B] The positions of the two studied breccia fabrics are shown on a Google Earth satellite image (Imagery ©2015 CNES/Astrium, Digital Globe, Map data ©2015 Google). The large-scale breccia fabric (Fig. 2A) has the edge point

coordinates A and B and the small scale breccia fabric (Fig. 2A) is located at point C.

Fig. 2: [A] The field panorama displays the studied outcrop and the two observed breccia fabrics referred to as large scale breccia fabric (LSB) and small scale breccia fabric (SSB). Both fabrics reveal differences in size, shape and clast/matrix characteristics. The dashed yellow line marks the sample transect for stable isotope and XRD analysis. [B] The schematic sketch illustrates the clast size distribution in the LSB fabric which is separated into area 1 and 2. Area 2 is located in the centre of the breccia and shows tens of meter wide blocks without brecciation features. The size of the clasts in area 1 is relatively homogenous and the entire fabric is brecciated. [C] The schematic sketch shows the shape of the SSB breccia fabric. In comparison to B, it is more irregular in shape and shows a decrease in the clast content towards the top. Non brecciated areas are preserved at the base of the SSB fabric. Explanations of symbols are valid for B and C.

Fig. 3: [A and B] The image on the left side shows the typical appearance of the LSB fabric present in the WNW part of area 1. The associated sketch on the right side illustrates the distribution of clasts and matrix present in [A]. The angular clasts reveal varying sizes and lack sorting with respect to the clast size. [C and D] The image (left side) shows the typical appearance of the LSB fabric present in the ENE part of area 1. Similar to [B] a wide spectrum of clast sizes can be observed in the digitized sketch on the right side. [E] The image displays the central part of the LSB fabric defined as area 1. The white lines indicate large

non brecciated blocks which often lack evidence for a displacement (left most block). [F] The image shows the typical appearance of DT2 dolomite in the outcrop captured under crossed nichols. The edges of crinoid columnals are often replaced by dolomite rhombs. [G] Early dolomite clasts often float in the DT2 dolomite matrix (captured under parallel nichols).

Fig. 4: The images [A] and [C] show the distribution of clasts in the SSB fabric. The sketches [B] and [D] presented on the right side illustrate the clast size and clast distribution as well as the matrix observed in [A] and [C]. In contrast to the LSB fabric large parts of the matrix have a limestone composition and only the top and edge parts of the breccias show a dolomitized matrix. [E] Stylolite suturs present within clasts often show different directions and terminate at the edge of the clasts. [F] Centimetre wide pipes are oriented in naerly bedding parallel directions and are filled with clasts.

Fig. 5: The base of the LSB fabric shows fractures aligned by dolomite halos [A]. The width of the halos is often increasing towards stratigraphically younger beds. [B] Vuges filled with calcite and dolomite float within the dolomite matrix or are present at the edge of clasts. In the matrix of the SSB fabric [C] finely laminated layers (white arrow) with crinoid debris occur. The bedding direction of these layers often deviates from the bedding planes of the host rock. Image [D] shows weathered celestite laths hosted in an undolomitized limestone matrix which is rich in fossils such as bivalve shells and crinoids. [E] The unbrecciated limestone matrix reveals a sharp border (red dashed line) with the brecciated SSB fabric. The unbrecciated fabric shows intense *Zoophycus*

bioturbations. Picture [F] shows dolomitized celestite laths present in a hand sample [D].

Fig. 6: A: The graph on the left side displays the oxygen and carbon isotope values of DT2 dolomite samples of the LSB breccia matrix and adjacent non brecciated dolomite fingers. The results of the surrounding non dolomitized limestone host rock and ED dolomite are plotted as well. The matrix of the LSB fabric reveals two different phases of DT2 dolomite. The graph on the right side shows all late diagenetic dolomite phases recognized in Permian host rocks in the Central Oman Mountains. DT 2 and Type 3 (DT3 P) dolomite samples presented in Vandeginste et al. (2015) are plotted, in order to show the consensus in the carbon and oxygen isotope values of DT2 dolomite samples compared to this study. B: The graphs show oxygen and carbon isotope values measured across the LSB fabric and adjacent parts of the DT2 dolomite fingers.

Figure 7: The six sketches display the suggested model for the formation of the LSB and SSB fabric observed in Wadi Sahtan. The breccia fabrics are assumed to represent a collapsed cavernous system either linked to a meteoric or a hypogenic karst.

References

Aigner, T., Dott, R.H., 1990. Processes and Patterns in Epeiric Basins: Special Issues. Elsevier.

Al-Husseini, M., 2006. Permian Arabian Tectono-Stratigraphic Chart. GeoArabia 11, 95-102.

Anderson, R.Y., Kirkland, D.W., 1980. Dissolution of salt deposits by brine density flow. Geology 8, 66-69.

Audra, P., D'Antoni-Nobecourt, J.-C., Bigot, J.-Y., 2010. Hypogenic caves in France. Speleogenesis and morphology of the cave systems. Bulletin de la Societe Geologique de France 181, 327-335.

Baud, A., Beauchamp, B., Richoz, S., 2012. A unique Permian–Triassic boundary section from the Neotethyan Hawasina Basin, Central Oman Mountains, International Conference on the Geology of the Arabian Plate and the Oman Mountains, Muscat, Sultanate of Oman.

Beckert, J., Vandeginste, V., John, C.M., 2015. Exploring the geological features and processes that control the shape and internal fabrics of late diagenetic dolomite bodies (Lower Khuff equivalent - Central Oman Mountains). Mar Petrol Geol.

Bendias, D., Koehrer, B., Obermaier, M., Aigner, T., 2013. Mid-Permian Khuff Sequence KS6: Paleorelief-influenced facies and sequence patterns in the Lower Khuff time-equivalent strata, Oman Mountains, Sultanate of Oman. GeoArabia 18, 135-178.

Beurrier, M., Béchennec, F., Hutin, G., Rabu, D., 1982-1985. Map Rustaq (NF40-3D). Sultanate of Oman. Ministry of Petroleum and Minerals. Directorate General of Minerals.

Botton-Dumay, R., Manivit, T., Massonnat, G., Gay, V., 2002. Karstic High Permeability Layers: Characterization and Preservation While Modeling Carbonate Reservoirs. Society of Petroleum Engineers.

Boudier, F., Bouchez, J.L., Nicolas, A., Cannat, M., Ceuleneer, G., Misseri, M., Montigny, R., 1985. Kinematics of oceanic thrusting in the Oman Ophiolite - Model of plate convergence. Earth and Planetary Science Letters 75, 215-222.

Breesch, L., Swennen, R., Vincent, B., Ellison, R., Dewever, B., 2010. Dolomite cementation and recrystallisation of sedimentary breccias along the Musandam Platform margin (United Arab Emirates). J Geochem Explor 106, 34-43.

Breton, J.P., Béchennec, F., Le Métour, J., Moen-Morel, L., Razin, P., 2004. Eoalpine (Cretaceous) evolution of the Oman Tethyan continental margin: insights from a structural study in Jabal Akhdar (Oman Mountains). GeoArabia 9, 41-58.

Callot, J.-P., Breesch, L., Guilhaumou, N., Roure, F., Swennen, R., Vilasi, N., 2010. Paleo-fluids characterisation and fluid flow modelling along a regional transect in Northern United Arab Emirates (UAE). Arab J Geosci 3, 413-437.

Chauvet, F., Dumont, T., Basile, C., 2009. Structures and timing of Permian rifting in the central Oman Mountains (Saih Hatat). Tectonophysics 475, 563-574.

Coy, G.A., 1997. Dolomitization of the Akhdar Group: The Arabian platform of Oman. Darwin College, Cambridge, United Kingdom, unpublished PhD thesis.

Dewit, J., Huysmans, M., Muchez, P., Hunt, D.W., Thurmond, J.B., Verges, J., Saura, E., Fernandez, N., Romaire, I., Esestime, P., Swennen, R., 2012. Reservoir characteristics of fault-controlled hydrothermal dolomite bodies: Ramales Platform case study. Geological Society, London, Special Publications 370, 83-109.

Dickson, J.A.D., 1966. Carbonate identification and genesis as revealed by staining. Journal of Sedimentary Research 36, 491-505.

Dublyansky, Y.V., 1995. Speleogenetic history of the Hungarian hydrothermal karst. Geo 25, 24-35.

Dublyansky, Y.V., 2000. Dissolution of carbonates by geothermal waters, in: Klimchouk, A., Palmer, A., Ford, D., Dreybrodt, W. (Eds.), Speleogenesis: Evolution of Karst Aquifers. National Speleological Society, Huntsville, Alabama, U.S.A.

Dublyansky, Y.V., Spoetl, C., 2015. Condensation-corrosion speleogenesis above a carbonate-saturated aquifer: Devils Hole Ridge, Nevada. Geomorphology 229, 17-29.

Fontana, S., Nader, F., Morad, S., Ceriani, A., Al-Aasm, I., 2010. Diagenesis of the Khuff Formation (Permian–Triassic), northern United Arab Emirates. Arab J Geosci 3, 351-368.

Frumkin, A., Gvirtzman, H., 2006. Cross-formational rising groundwater at an artesian karstic basin: the Ayalon Saline Anomaly, Israel. Journal of Hydrology 318, 316-333.

Frumkin, A., Zaidner, Y., Na'aman, I., Tsatskin, A., Porat, N., Vulfson, L., 2015. Sagging and collapse sinkholes over hypogenic hydrothermal karst in a carbonate terrain. Geomorphology 229, 45-57.

Hacker, B.R., 1994. Rapid emplacement of young oceanic lithosphere - Argon geochronology of the Oman Ophiolite Science 265, 1563-1565.

Hajikhazemi, E., Al-Aasm, I.S., Coniglio, M., 2010. Karst controlled diagenesis: An example from the Middle Cretaceous Sarvak Formation, S.W. Iran. Geological Society of London, Special Publication 330, 253-272.

Hamilton, J., Ford, D., 2002. Karst geomorphology and hydrogeology of the Bear Rock Formation-A remarkable dolostone and gypsum megabreccia in the continous permafrost zone of Northwest Territories, Canada. Carbonates Evaporites 17, 114-115.

Hill, C.A., 1990. Sulfuric acid spelogenesis of Carlsbad Cavern and its relationship to hydrocarbons, Delaware Basin, New Mexico and Texas. Aapg Bulletin 74, 1685-1694.

Hoefs, J., 2004. Stable isotope geochemistry, 5th ed. Springer, Berlin.

Horton, T.W., Atkinson, L., Oze, C., 2012. Hydrothermal carbonate geochemsitry of the Ngatamariki subsurface reservoir, New Zealand, Thirty-Seventh workshop on geothermal reservoir engineering, Stanford University.

Hulen, J.B., Nielson, D.L., 1988. Hydrothermal brecciation in the Jemez fault zone, Valles Caldera, New Mexico: Results from continental Scientific Drilling Program core hole VC-1. Journal of Geophysical Research: Solid Earth 93, 6077-6089.

Husseini, M.I., Husseini, S.I., 1990. Origin of the Infracambrian Salt Basins of the Middle East. Geological Society, London, Special Publications 50, 279-292.

Jébrak, M., 1997. Hydrothermal breccias in vein-type ore deposits: A review of mechanisms, morphology and size distribution. Ore Geology Reviews 12, 111-134.

Kempe, S., Al-Malabeh, A., Henschel, H.-V., 2009a. Hypogene karstification in Jordan (Bergish-Daher Cave, Uwaiyed Cave, Beer Al-Malabeh Sinkhole), in: Klimchouk, A., Ford, D. (Eds.), Hypogene speleogenesis and karst hydrogeology of artesian basins. Ukrainian Institute of Speleology and Karstology, Simferopol.

Kempe, S., Dirks, H., Bauer, I., 2009b. Hypogene karstification in Saudi Arabia (Layla Lake Sinkholes, Ain Heeth Cave), in: Klimchouk, A., Ford, D. (Eds.), Hypogene speleogenesis and karst hydrogeology of artesian basins. Ukrainian Institute of Speleology and Karstology, Simferopol.

Keulen, N., Heilbronner, R., Stünitz, H., Boullier, A.-M., Ito, H., 2007. Grain size distributions of fault rocks: A comparison between experimentally and naturally deformed granitoids. Journal of Structural Geology 29, 1282-1300.

Kim, S.T., Mucci, A., Taylor, B.E., 2007. Phosphoric acid fractionation factors for calcite and aragonite between 25 and 75°C. Chemical Geology 246, 135-146.

Klimchouk, A., 2011. Hypogene speleogenesis: Hydrogeological and morphometric perspective, 2nd ed. National Cave and Karst Reserach Institute, Carlsbad.

Koehrer, B., Aigner, T., Holger, F., Pöppelreiter, M., 2012. Middle to Upper Khuff (Sequences KS1 to KS4) outcrop-equivalents in the Oman Mountains: Grainstone architecture on a subregional scale. GeoArabia 17, 59-104.

Koehrer, B., Aigner, T., Poeppelreiter, M., 2011. Field-scale geometries of Upper Khuff reservoir geobodies in an outcrop analogue (Oman Mountains, Sultanate of Oman). Petroleum Geoscience 17, 3-16.

Koehrer, B., Zeller, M., Aigner, T., Poeppelreiter, M., Milroy, P., Forke, H., Al-Kindi, S., 2010. Facies and stratigraphic framework of a Khuff outcrop equivalent: Saiq and Mahil formations, Al Jabal al-Akhdar, Sultanate of Oman. Geoarabia 15, 91-156.

Lapponi, F., Casini, G., Sharp, I., Blendinger, W., Fernández, N., Romaire, I., Hunt, D., 2011. From outcrop to 3D modelling: a case study of a dolomitized carbonate reservoir, Zagros Mountains, Iran. Petroleum Geoscience 17, 283-307.

López-Horgue, M.A., Iriarte, E., Schröder, S., Fernández-Mendiola, P.A., Caline, B., Corneyllie, H., Frémont, J., Sudrie, M., Zerti, S., 2010. Structurally controlled hydrothermal dolomites in Albian carbonates of the Asón valley, Basque Cantabrian Basin, Northern Spain. Mar Petrol Geol 27, 1069-1092.

Lucia, J.F., 1995. Lower Paleozoic cavern development, collapse, and dolomitization, Franklin Mountains, El Paso, Texas. American Association of Petroleum Geologists.

McKean, T.J., 2012. Multiphase dolomite: characterization, implications and prediction - Permian Khuff equivalent, Wadi Mistal, Northern Oman. Imperial College London, UK, Unpublished M. Sc. thesis.

Mort, K., Woodcock, N.H., 2008. Quantifying fault breccia geometry: Dent Fault, NW England. Journal of Structural Geology 30, 701-709.

Osborne, R.A.L., 2001. Non-meteoric speleogensis: Evidence from Eastern Australia, 13th International Congress of Speleology, Brasil.

Pillevuit, A., 1993. Les blocs exotiques du Sultanat d'Oman : évolution paléogéographique d'une marge passive flexurale, Faculté des sciences. Institut de géologie et de paléontologie. Université de Lausanne, Mémoires de géologie (Lausanne), p. 249.

Quye-Sawyer, J., Vandeginste, V., Johnston, K.J., 2015. Application of handheld energy-dispersive X-ray fluorescence spectrometry to carbonate studies: opportunities and challenges. Journal of Analytical Atomic Spectrometry 30, 1490-1499.

Rabu, D., Béchennec, F., Beurrier, M., Hutin, G., 1982-1983. Map Nakhl (NF40-3E). Sultanate of Oman. Ministry of Petroleum and Minerals. Directorate General of Minerals.

Radke, B.M., Mathis, R.L., 1980. On the formation and occurrence of saddle dolomite. Journal of Sedimentary Research 50, 1149-1168.

Reuning, L., Schoenherr, J., Heimann, A., Urai, J.L., Littke, R., Kukla, P.A., Rawahi, Z., 2009. Constraints on the diagenesis, stratigraphy and internal dynamics of the

surface-piercing salt domes in the Ghaba Salt Basin (Oman): A comparison to the Ara Group in the South Oman Salt Basin GeoArabia 14, 83-120.

Rosenbaum, J., Sheppard, S.M., 1986. An isotopic study of siderites, dolomites and ankerites at high temperatures. Geochimica et Cosmochimica Acta 54, 603-610.

Ruban, D.A., Al-Husseini, M.I., Iwasaki, Y., 2007. Review of Middle East Paleozoic plate tectonics. GeoArabia 12, 35-56.

Salvati, R., Sasowsky, I.D., 2002. Development of collapse sinkholes in areas of groundwater discharge. Journal of Hydrology 264, 1-11.

Searle, M., Cox, J., 1999. Tectonic setting, origin, and obduction of the Oman ophiolite. Geological Society of America Bulletin 111, 104-122.

Searle, M.P., 2007. Structural geometry, style and timing of deformation in the Hawasina window, Al Jabal al Akhdar and Saih Hatat culminations, Oman mountains. Geoarabia 12, 99-130.

Sharland, P.R., Raymond Archer, Casey, D.M., Davies, R.B., Hall, S.H., Heward, A.P., Horbury, A.D., Simmons, M.D., 2001. Arabian Plate Sequence Stratigraphy. GeoArabia.

Sharp, I., Gillespie, P., Morsalnezhad, D., Taberner, C., Karpuz, R., VergéS, J., Horbury, A., Pickard, N., Garland, J., Hunt, D., 2010. Stratigraphic architecture and fracture-controlled dolomitization of the Cretaceous Khami and Bangestan groups: an outcrop case study, Zagros Mountains, Iran. Geological Society, London, Special Publications 329, 343-396.

Smith, A.G., 2012. A review of the Ediacaran to Early Cambrian ('Infra-Cambrian') evaporites and associated sediments of the Middle East. Geological Society, London, Special Publications 366, 229-250.

Spötl, C., Pitman, J.K., 2009. Saddle (Baroque) Dolomite in Carbonates and Sandstones: A Reappraisal of a Burial-Diagenetic Concept, Carbonate Cementation in Sandstones. Blackwell Publishing Ltd., pp. 437-460.

Stampfli, G.M., Borel, G.D., 2002. A plate tectonic model for the Paleozoic and Mesozoic constrained by dynamic plate boundaries and restored synthetic oceanic isochrons. Earth and Planetary Science Letters 196, 17-33.

Stern, R.J., Johnson, P., 2010. Continental lithosphere of the Arabian Plate: A geologic, petrologic, and geophysical synthesis. Earth-Science Reviews 101, 29-67.

Strohmenger, C.J., Alway, R.H.S., Broomhall, R.W., Hulstrand, R.F., Al-Mansoori, A., Abdalla, A.A., Al-Aidarous, A., 2002. Sequence stratigrapgy of the Khuff Formation comparing subsurface and outcrop data (Arabian Plate, U.A.E.). Society of Petroleum Engineers (SPE).

Tisato, N., Sauro, F., Bernasconi, S.M., Bruijn, R.H.C., De Waele, J., 2012. Hypogenic contribution to speleogenesis in a predominant epigenic karst system: A case study from the Venetian Alps, Italy. Geomorphology 151–152, 156-163.

Vandeginste, V., John, C.M., Beckert, J., 2015. Diagenetic Geobodies: Fracture-Controlled Burial Dolomite in Outcrops From Northern Oman. Society of Petroleum Engineers (SPE) 18, 84-93.

Vandeginste, V., John, C.M., Cosgrove, J.W., Manning, C., 2014. Dimensions, texture-distribution, and geochemical heterogeneities of fracture–related dolomite geobodies hosted in Ediacaran limestones, northern Oman. AAPG Bulletin 98, 1789-1809.

Vandeginste, V., John, C.M., van de Flierdt, T., Cosgrove, J.W., 2013. Linking process, dimension, texture, and geochemistry in dolomite geobodies: A case study from Wadi Mistal (northern Oman). AAPG Bulletin 97, 1181-1207.

Villey, M., de Gramont, X., Le Métour, J., 1982-1985. Map Fanjah (NF40-3F). Sultanate of Oman. Ministry of Petroleum and Minerals. Directorate General of Minerals.

Walz, L., Aigner, T., Koehrer, B., 2013. Khuff Sequence KS5 outcrop-equivalents in the Oman Mountains, Sultanate of Oman: Variations to the simple "layer-cake" stratigraphy. GeoArabia 18, 179-218.

Weidlich, O., 2010. Meteoric diagenesis in carbonates below karst unconformities: heterogeneity and control factors. Geological Society, London, Special Publications 329, 291-315.

Weidlich, O., Bernecker, M., 2011. Biotic carbonate precipitation inhibited during the Early Triassic at the rim of the Arabian Platform (Oman). Palaeogeography, Palaeoclimatology, Palaeoecology 308, 129-150.

Woodcock, N.H., Omma, J.E., Dickson, J.A.D., 2006. Chaotic breccia along the Dent Fault, NW England: implosion or collapse of a fault void? Journal of the Geological Society 163, 431-446.

Wright, V.P., Woodcock, N.H., Dickson, J.A.D., 2009. Fissure fills along faults: Variscan examples from Gower, South Wales [electronic version]. Cambridge University Press.

Ziegler, M.A., 2001. Late Permian to Holocene paleofacies evolution of the Arabian Plate and its hydrocarbon occurrences. GeoArabia 6, 445-504.

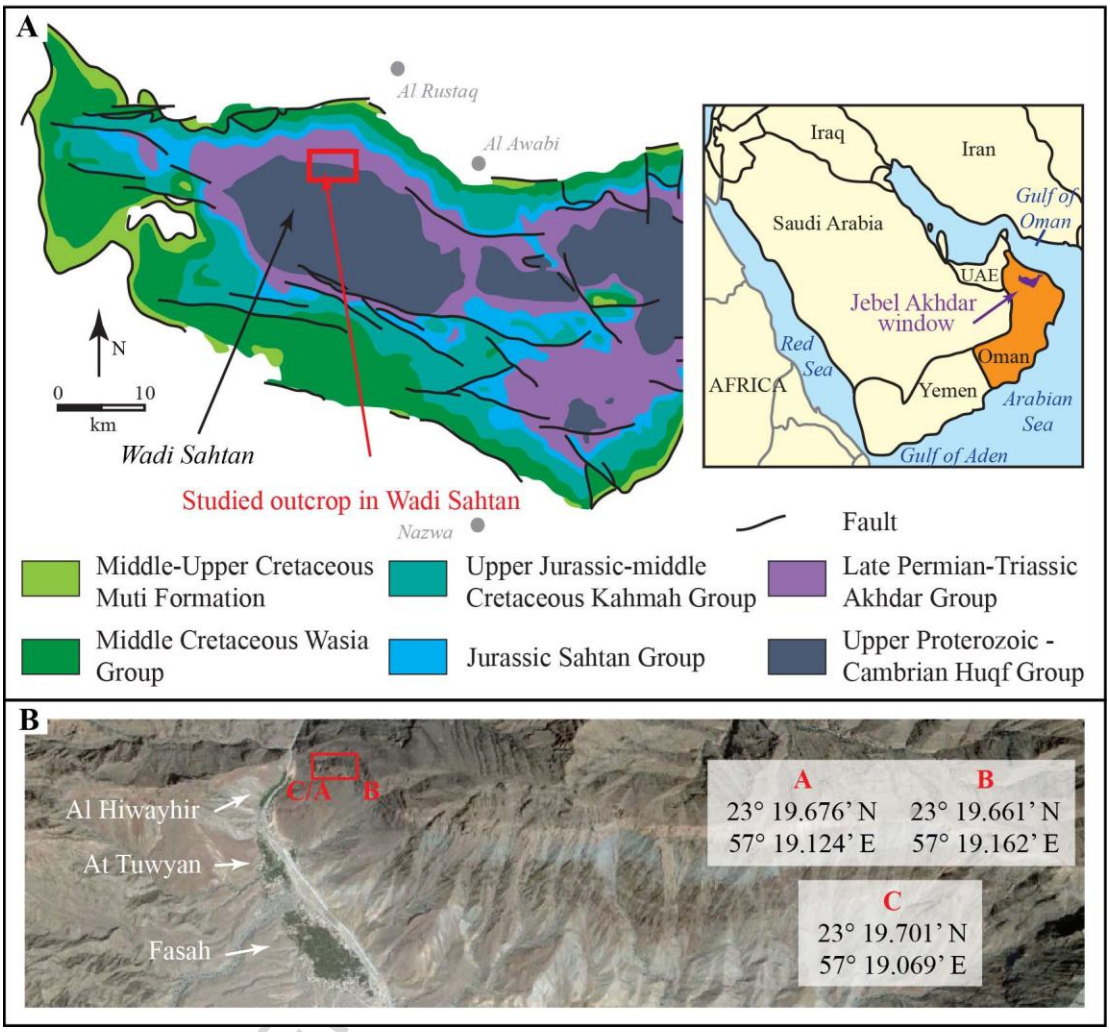

Figure 1

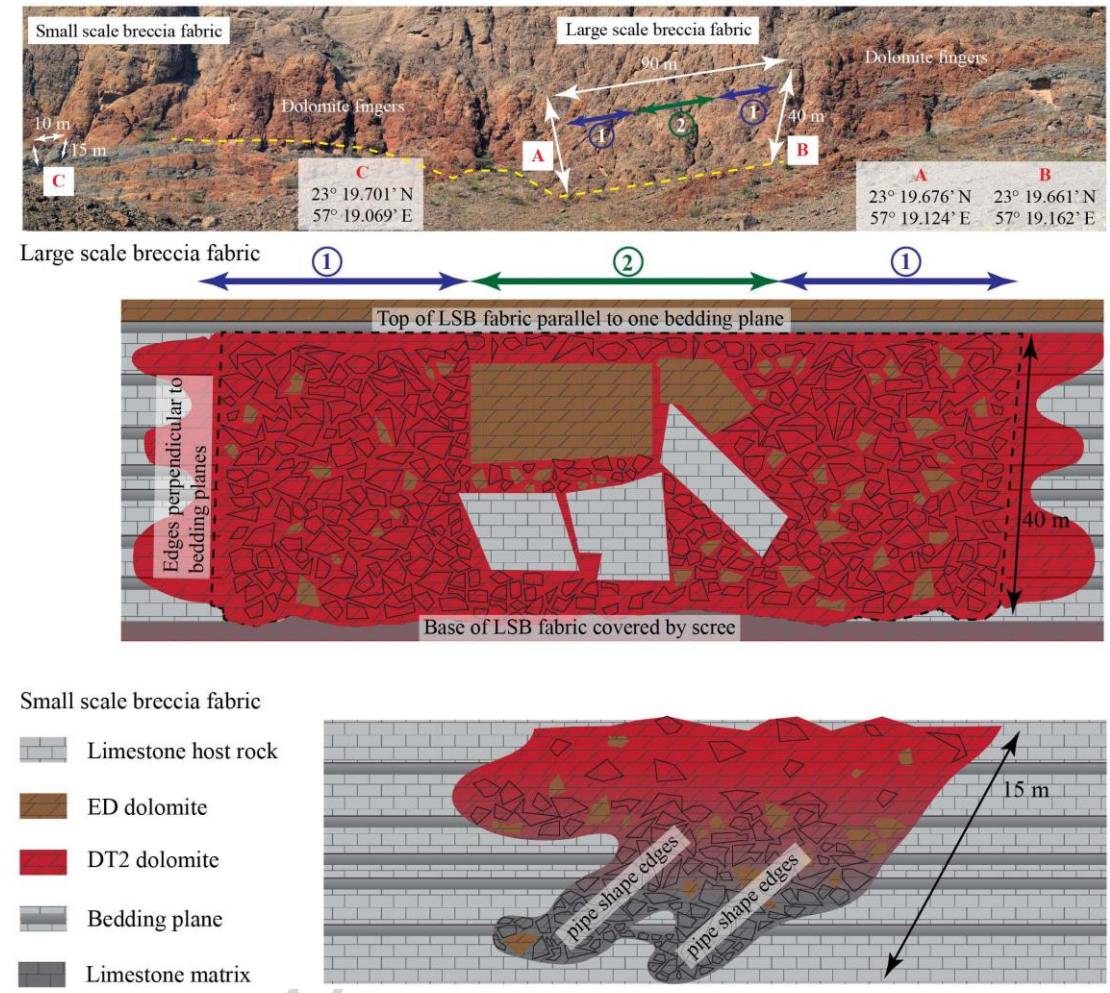

Figure 2

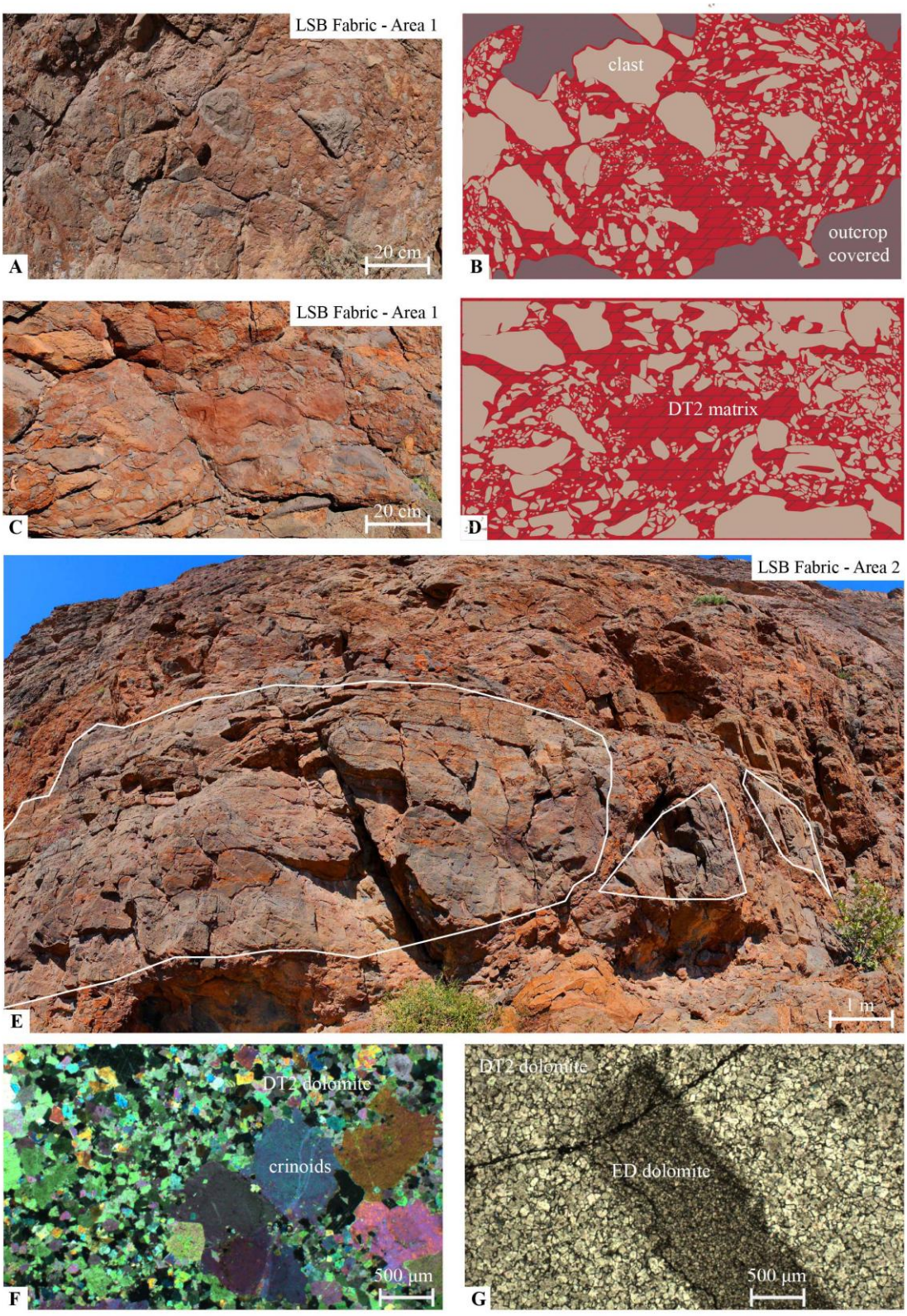
LSB Fabric - Area 1
20 cm
A
clast
outcrop covered
B
LSB Fabric - Area 1
20 cm
C
DT2 matrix
D
LSB Fabric - Area 2
1 m
E
DT2 dolomite
crinoids
500 µm
F
DT2 dolomite
ED dolomite
500 µm
G

Figure 3

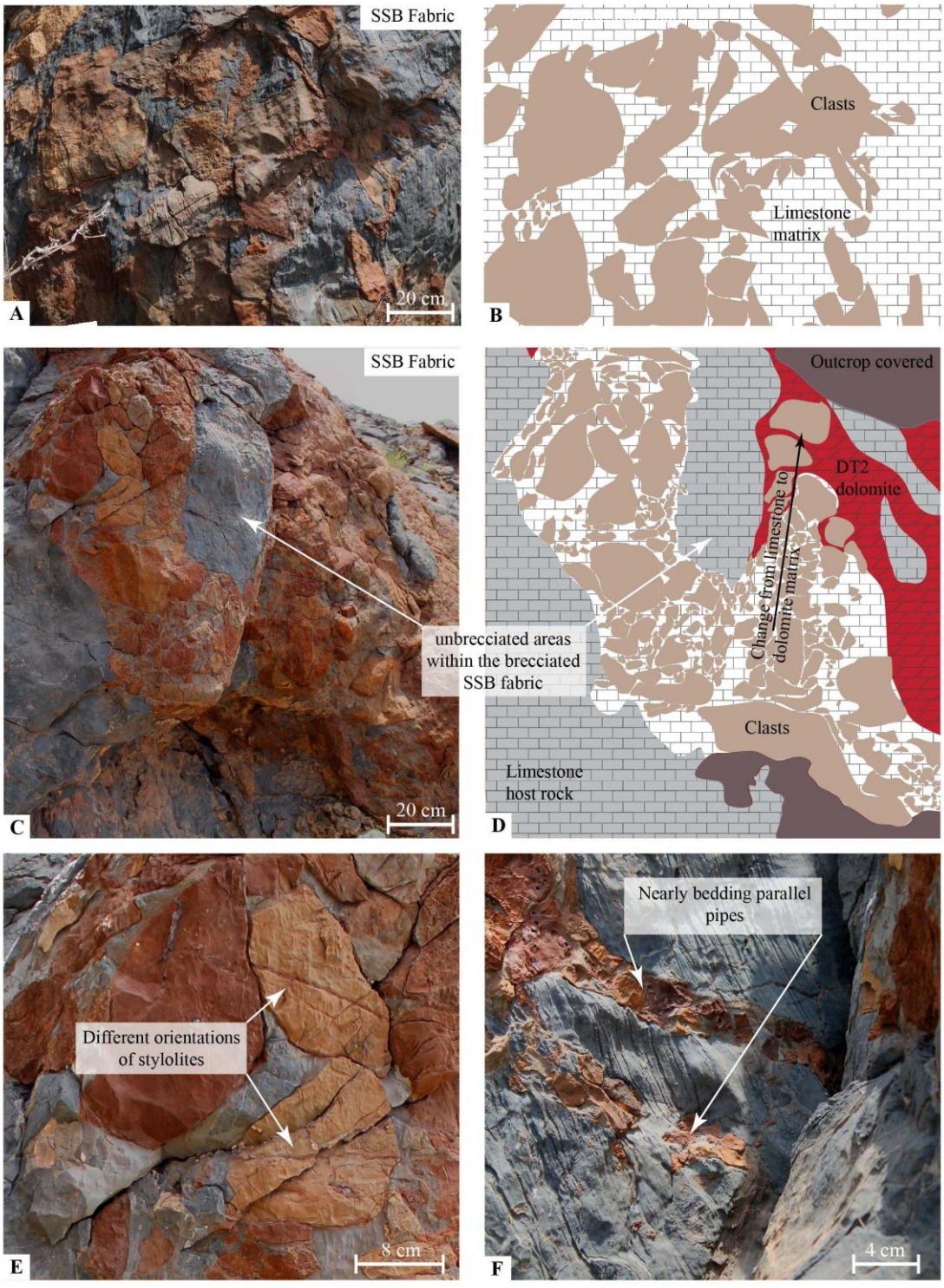

Figure 4

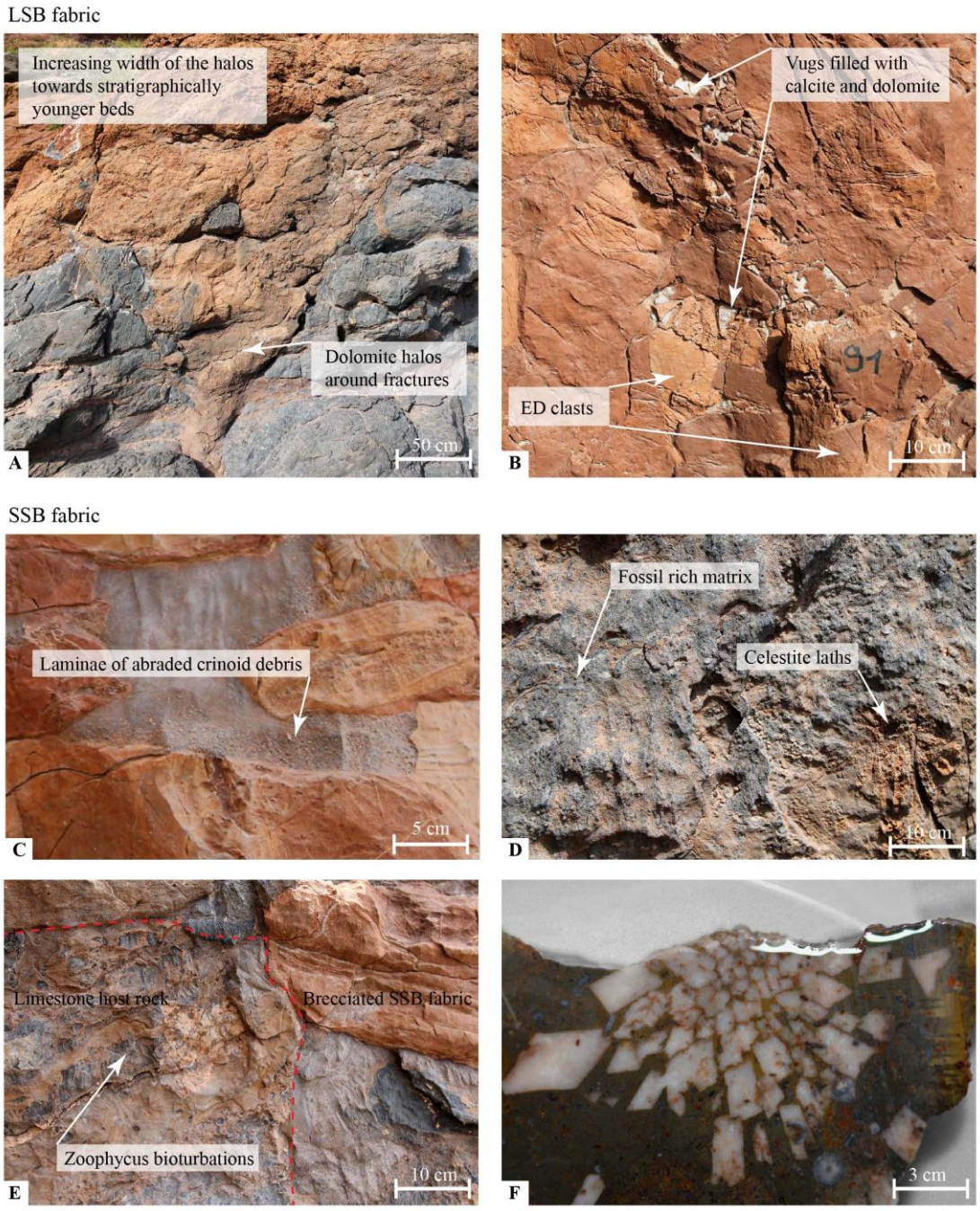

Figure 5

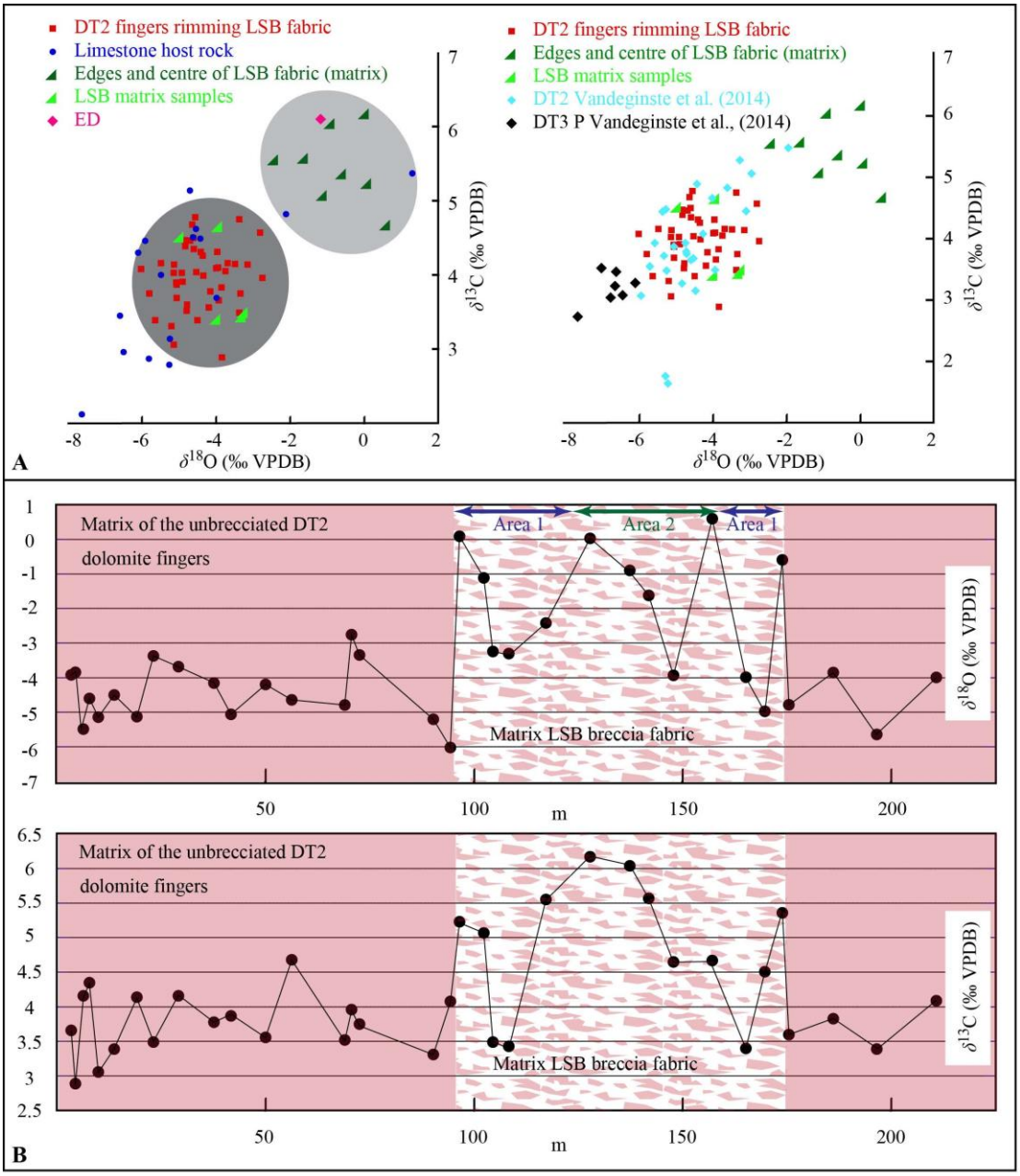

Figure 6

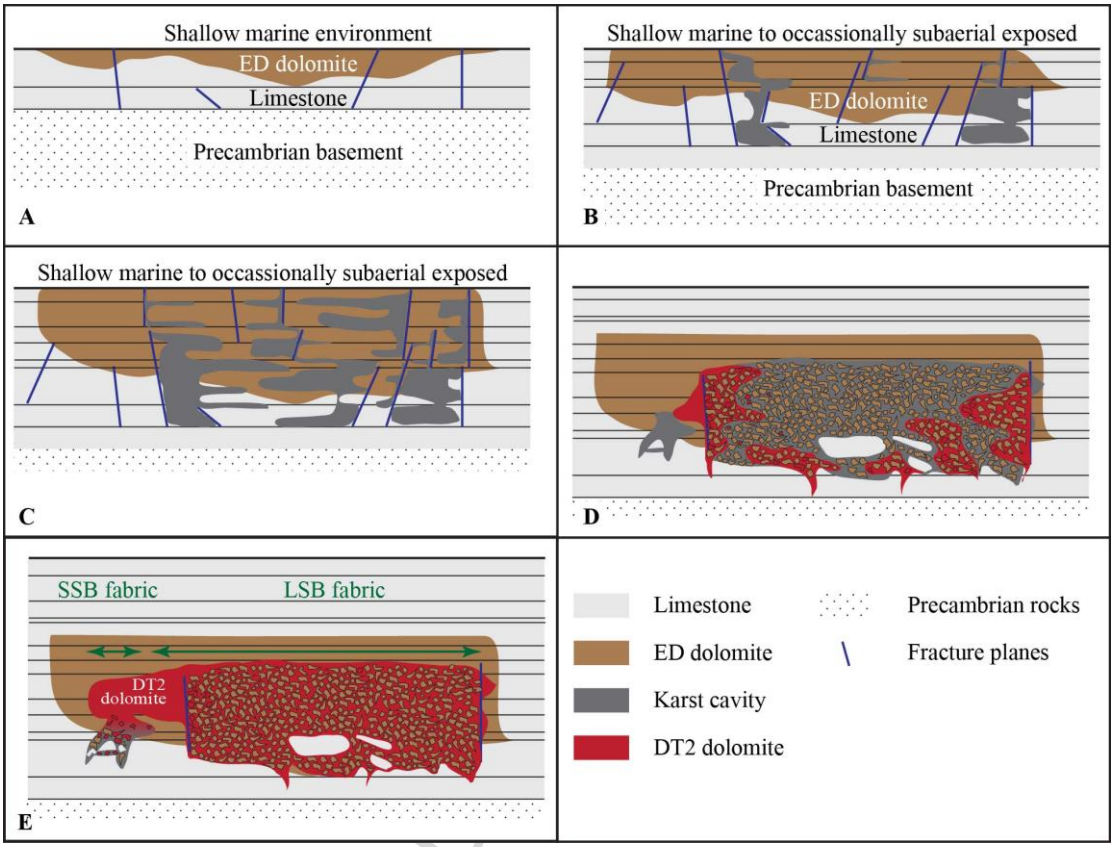

Figure 7